E83-10094
CR-169604

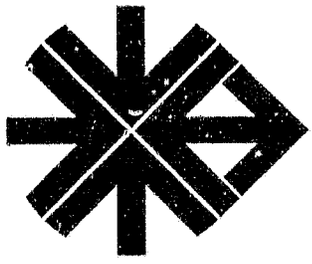

(E83-10094) EQUIVALENT SOURCE MODELING OF THE MAIN FIELD USING MAGSAT DATA Final Report (Business and Technological Systems, Inc.) 38 p HC A03/MF A01 CSCL 08N

N83-14601

Unclas
G3/43 00094

BTS

BUSINESS AND TECHNOLOGICAL SYSTEMS, INC.

BTS33-82-60/br
C142FR

MAY 1982

Prepared By
BUSINESS AND TECHNOLOGICAL SYSTEMS, INC.
Aerospace Building, Suite 440
10210 Greenbelt Road
Seabrook, Maryland 20706

EQUIVALENT SOURCE MODELING OF THE MAIN FIELD USING MAGSAT DATA.

by
M. A. Mayhew
R. H. Estes

FINAL REPORT
Contract NAS5-26047

Prepared For
NATIONAL AERONAUTICS AND SPACE ADMINISTRATION
Goddard Space Flight Center
Greenbelt, Maryland 20771

TABLE OF CONTENTS

1.0 INTRODUCTION

2.0 METHODOLOGY

3.0 RESULTS

3.1 Single-Epoch Models

3.2 Time-Dependent Models

4.0 CONCLUSIONS

5.0 REFERENCES

FIGURES

TABLES

APPENDIX - SOFTWARE DESCRIPTION AND FLOW CHART

EQUIVALENT SOURCE MODELING OF THE MAIN FIELD USING MAGSAT DATA

M. A. Mayhew and R. H. Estes
BTS, Inc. Seabrook, MD 20706

Abstract

An iterative least squares estimation algorithm with the capability for including a priori statistical information has been implemented to recover multiple magnetic dipole models of the Earth's main magnetic field. The dipoles are fixed to a specified radius at or below the core-mantle boundary and centered on equal area blocks. The algorithm can solve for dipole magnitudes only (fixed orientations), or allow full freedom of orientation and solve for vector components. External field parameters and observatory anomaly biases can also be estimated simultaneously. Time dependence is modeled using first time derivatives for dipole vector components. Single-epoch and time dependent dipole models are derived using MAGSAT and observatory annual means data. Equivalent spherical harmonic representations are computed in closed form from the dipole models and compared with truncated spherical harmonic models estimated in the standard way from the same data sets. In particular, a 21° spatial resolution model based on 93 dipoles is computed based on observatory annual means data from 1974 through 1977 and a selected MAGSAT data set and is compared with candidate IGRF 1975 models and their 1980 secular variation. The equivalent dipole source representation is shown to be comparable to the standard spherical harmonic approach in accuracy and, for high resolution models, to be superior in computational efficiency for field model evaluation when three degree-of-freedom unconstrained dipoles are utilized. Fixing of the dipole positions results in rapid convergence of the dipole solutions for single-epoch models. For time dependent models, a sufficiently long time interval of data must be

available or a priori values and statistics available for the derivatives to achieve convergence. In contrast to standard spherical harmonic models based on the same data, the correlation structure of dipole magnetic moment derivatives with the constant magnetic moment parameters is small, indicating the ability to strongly separate the constant field and the secular variation. The dipole equivalent source approach for the main field was found not to be effective as a technique for distinguishing core and crustal fields.

1.0 INTRODUCTION

The equivalent source technique is a conceptually simple means of describing potential fields which has been widely applied in exploration geophysics (e.g. Dampney, 1969), in modeling long wavelength satellite magnetic anomalies (Mayhew, 1979), and in modeling the core field (see review by Sterns and Alldredge, 1973). The method consists of setting up an internal arrangement of dipoles and adjusting their magnetic moments (and in some applications their positions) such that the synthetic field arising from them collectively best fits a set of observations of the field. A number of authors have attempted to apply the equivalent source technique to modeling of the main field and its secular change. McNish (1940) and Lowes and Runcorn (1951) used graphical approximation techniques for this purpose. Alldredge and Hurwitz (1964) and Alledredge and Sterns (1969) treated the problem using inverse theory and with the benefit of computers. The goal of the modern studies has been to gain insight into the physics of core field generation by examination of the behavior of modeled sources: for example, the fields of radial dipoles can be taken to approximate the fields of current loops. Some authors (e.g. Peddie, 1979) have used expressions for current loops directly.

In most of these studies, the angular coordinates and radial distance of the dipoles are treated as variables in addition to the dipole moments, and herein lies the difficulty of this approach to core field modeling. The function expressing the dipole field is non-linear in the geographic variables, and this leads to a non-linear inverse problem. Many iterations through a given data set are required for convergence; for example, 180 iterations were required to fit 21 dipoles to the 1955 Finch-Leaton model of the field (Stearns and Alldredge, 1973), and 25,000 iterations were required to fit the 1966 IGRF secular change field (Alldredge and Stearns, 1969). Furthermore, convergence was not achieved at all unless good starting parameter estimates were available. Previous approaches have sought to reproduce existing field

models expressed in spherical harmonics. A current function (Chapman and Bartels, 1940) is derived for a thin shell within the core from the spherical harmonic coefficients, and the starting positions of the dipoles are taken to be the current foci. The inapplicability of this approach when one is trying to generate a field model from scratch is obvious. Further, there is no way of knowing before hand how many dipoles are required to properly model the field.

Our previous work in magnetic dipole analysis has been aimed at modeling the long wavelength anomalies in the total magnetic field from satellite data. An array of dipoles is laid out in equal area at the Earth's surface in a specific region, and the magnetic moments of the dipoles adjusted by a least squares procedure so as to collectively give rise to a field which best fits that observed over the region. For this (essentially geologic) application, the dipoles are constrained to lie in the direction of the main field at the dipole position. In this study we have applied the methodology and the associated software to modeling the core field. We have experimented with fitting the main field using different numbers of equivalent sources at fixed radii at and within the core-mantle boundary. By fixing the radius for a given series of runs, we avoid the convergence problems which result from the extreme non-linearity of the problem when dipole positions are allowed to vary. The study had three main goals: 1) to compare the equivalent source approach with the standard spherical harmonic approach for modeling the main field in terms of accuracy and computational efficiency, 2) to examine the possibility of distinguishing core and crustal fields with this approach, and 3) to see whether a systematic distribution of solution parameters, possibly indicative of fluid motions, could be described, and if so what dipole density is required to resolve the pattern.

2.0 METHODOLOGY

Mayhew (1978) and Mayhew and Estes (1980) have given the expressions for the anomaly components and the anomaly in the total field due to a dipole having arbitrary position and orientation at an arbitrary external position. The magnetic potential at an external point of a dipole of moment $\bar{M}$ is $V = -\bar{M} \cdot \nabla(1/\ell)$, where ℓ is the distance between the dipole and the external point; the associated vector field is $\bar{F} = -\nabla V$. Let θ be colatitude, ϕ be longitude, and r be the radial distance, and let $\bar{M}$ have components (M_r, M_θ, M_ϕ). Then V may be written

$$V = [M_r(rA-r') - M_\theta rB + M_\phi rC]/\ell^3 , \qquad (1)$$

where

$$\ell = (r^2 + r'^2 - 2rr'A)^{1/2}$$

$$A = \cos\theta \cos\theta' + \sin\theta \sin\theta' \cos(\phi-\phi')$$

$$B = \cos\theta \sin\theta' + \sin\theta \cos\theta' \cos(\phi-\phi')$$

$$C = \sin\theta \sin(\phi-\phi') .$$

Primed variables refer to the dipole position, unprimed to the external position. Then

$$\bar{F} = -\left(\frac{\partial}{\partial r} , \frac{\partial}{r\partial\theta} , \frac{\partial}{r\sin\theta\partial\phi}\right) V = (F_r, F_\theta, F_\phi) \qquad (2)$$

The components of $\overline{F}$ are obtained by straightforward differentiation, and are complicated functions of the geographic coordinates and the components of the magnetic moment. If the dipole has a radial orientation the expressions for the components simplify; they are given by Alldredge and Hurwitz (1964).

The goal of the analysis is to estimate values for the magnetic moments (M_r, M_θ, M_ϕ) for all dipoles from observations of the total field and its components. A software system (see Appendix) which is an elaboration of our previous equivalent source modeling software has been developed for this purpose. It uses an iterative least squares algorithm with the capability for a priori information which has been described in some detail by Mayhew and Estes (1980). The dipoles are set by user input to a specified radius within the earth, and are centered on nearly equal area blocks. The system has the option to solve for either the dipole magnitudes only (with the dipole orientations constrained to a preselected direction), or to allow full freedom of orientation for the dipoles and solve for the three components. The procedure for obtaining an approximate equal area distribution of dipole locations was obtained by use of an icosahedron, a regular polyhedron with 20 equilateral triangular faces, inscribed in a sphere, with the edges radially projected onto the sphere forming "spherical polyhedrons." The spherical icosahedron is the division of the sphere having the greatest number of regular pieces, and forms the base on which a nearly uniform distribution of points on the sphere may be defined. The following sets of points defining dipole locations have been implemented:

number of points	12	42	92	162
angular separation	64°	32°	21°	16° .

When the dipole directions are unconstrained there are three parameters to be estimated per dipole, but only one per dipole when the direction is constrained radially, since in that case $M_\theta = M_\phi = 0$. Secular variation is modeled by making each dipole magnetic moment component a linear function of time. This doubles the number of parameters for a given problem at a single epoch. An iterative technique is required for this problem when scalar magnetometer data is utilized due to the non-linearity introduced for this data type. The inversion problem is linear, however, for B_r, B_θ, B_ϕ data.

The set of simultaneously estimated parameters has been further extended in two ways. First, on option a set of three external field parameters expressed as spherical harmonic coefficients $\bar{g}_{10}$, $\bar{g}_{11}$, $\bar{h}_{11}$ can be computed. Second, also on option, observatory anomaly biases can be estimated at each observatory when annual means data is used (Langel, Estes and Mead, 1982).

The spherical harmonic representation of a given dipole distribution may be expressed in closed form. Let

$$V(r,\theta,\lambda) = \bar{a} \left| \sum_{n=1}^{\infty} \left(\frac{\bar{a}}{r}\right)^{n+1} \sum_{m=0}^{n} \left(g_{nm}\cos m\lambda + h_{nm}\sin m\lambda\right) P_{nm}(\cos\theta) \right.$$
$$\left. + \left(\frac{r}{\bar{a}}\right)\left(\bar{g}_{10}P_{10}(\cos\theta) + \left(\bar{g}_{11}\cos\lambda + \bar{h}_{11}\sin\lambda\right) P_{11}(\cos\theta)\right) \right| \qquad (3)$$

be the scalar potential of the main field where the Legendre polynomials are Schmidt normalized. The last term represents that portion of the

potential originating from sources outside of the sphere of radius $\bar{a}$ (three parameter external field model). The magnetic field is then

$$\bar{F} = -\nabla V \quad .$$

Consider the set of $\{j\}$ dipoles, where the i^{th} dipole is described by a source vector

$$M_{r_i},\ M_{\theta_i},\ M_{\phi_i}$$

and a spatial position

$$r_i,\ \theta_i,\ \phi_i \ .$$

The spherical harmonic coefficients are given (in Schmidt normalized form) by

$$g_{nm} = (\bar{a})^{-(n+2)} \sum_{i=1}^{\{j\}} r_i^{n-1} \left[n\, M_{r_i}\, P_{nm}(\cos\theta_i) \cos m\lambda_i \right.$$

$$\left. + M_{\theta_i} \frac{\partial P_{nm}(\cos\theta_i)}{\partial\theta} \cos m\lambda - m\, M_{\lambda_i}\, P_{nm}(\cos\theta_i) \frac{\sin m\lambda_i}{\sin\theta_i} \right] \qquad (4)$$

$$h_{nm} = (\bar{a})^{-(n+2)} \sum_{i=1}^{\{j\}} r_i^{n-1} \left[n\, M_{r_i}\, P_{nm}(\cos\theta_i) \sin m\lambda_i \right.$$

$$\left. + M_{\theta_i} \frac{\partial P_{nm}(\cos\theta_i)}{\partial\theta} \sin m\lambda_i + m\, M_{\lambda_i}\, P_{nm}(\cos\theta_i) \frac{\cos m\lambda_i}{\sin\theta_i} \right] \quad .$$

The coefficients may be calculated up to any order. The spatial power spectral content of the expansion is given by the relation (Lowes, 1966, 1974)

$$S_n = (N+1) \left[g_{no}^2 + \sum_{m=1}^{n} (g_{nm}^2 + h_{nm}^2) \right] \quad . \qquad (5)$$

3.0 RESULTS

Several main field solutions have been derived for various numbers of dipoles arranged on equal area projections at the core-mantle boundary. In these various solutions, the dipoles have been either fixed radially or allowed complete freedom of orientation, and have been modeled with and without time dependence and with and without the addition of a geocentric dipole (giving three additional parameters).

3.1 Single-epoch Models

Based on the MGST(6/80) data set of quiet November 5 and 6, 1979, MAGSAT data (Langel et al, 1980), several dipole models identified in Table I have been derived. The models for which the dipoles are constrained radially have a single degree of freedom per dipole, while the unconstrained models have three degrees of freedom per dipole. The inclusion of the geocentric dipole significantly improved the rms error of the 32° dipole density solution. The direction of the geocentric dipole moment from the model was within 10° of that calculated from the first degree spherical harmonic terms of MGST(6/80), while the magnitude was greater by approximately 4%. The magnitude of the solution geocentric dipole dominated those of the core/mantle boundary by an order of magnitude. The inclusion of the geocentric dipole in the 21° dipole density solution of model 4 showed no improvement in the fit to the data over model 3 and the geocentric dipole showed no closer agreement to the first degree terms of MGST(6/80) than did that of the 32° dipole density solution. All parameters in these solutions were strongly observable in the least squares estimation, with standard errors from three to four orders of magnitude smaller than the magnitude of the parameters. The coefficients of the spherical harmonic representation given by Equation (4) for models 3, 4 and 5 from Table I showed differences of less than 1 nT (nanotesla) when compared with MGST(6/80) though degree and order ten. The spatial power spectra computed from spherical harmonic

expansions of the dipole models were analyzed relative to crustal and core content. Figure 1 displays the power spectra for one of the dipole models and MGST(10/81), a spherical harmonic model based on MAGSAT data through degree and order 23 (Langel and Estes, 1982a).

The cause of the apparent bulge in the power spectrum for Dipole Model #4 (Figure 1) was investigated via a simulation. The simulation consisted of generating synthetic data at exactly the same spatial locations as the MGST(6/80) data set used in the equivalent dipole source models (a "pseudo-data set"), with the "data" consisting of measurements due to a crustal field plus a geocentric dipole only. The crustal field model used was a global equivalent source model based on POGO data (R. A. Langel, personal communication) which was expanded to degree and order 40 in spherical harmonics to analyze its spectral character, as well as to generate the synthetic data. The spectrum of the synthetic crustal field is undoubtedly biased at low order, since ultra-long wavelength trends were removed from the POGO data in generating the crustal equivalent source model. The work of Meyer et al (personal communication) predicts a white spectrum down to very low order. The distortion of the equivalent source spectrum does not, however, invalidate certain inferences which can be made from the results of the simulation. Least squares fits were made to the pseudo-data set with a single geocentric dipole and with a geocentric dipole plus dipoles of 32°x32° and 21°x21° density at the core/mantle boundary. The results for cases with and without noise are given in Table II, and the spectra of selected results are given in Figure 2. The results seem to indicate that the beginning of the bump in the spectrum of Dipole Model #4 in Figure 1 is due to crustal influence, while the departure of the spectrum from that of MGST(10/81) around expansion order 17 is due to the resolution limits of the dipole density (i.e., $\frac{360°}{21°} \cong 17$).

Time-dependent Models

Dipole solution models have been obtained with both 32° and 21° resolutions based on a quiet (K_p<1⁻) MAGSAT data set extending over four months (November 5, 1979 - March 15, 1980). Time dependence was modeled using first time derviatives for the dipole magnetization vector components, which doubles the total number of parameters in the solution. The solutions displayed a very slow convergence in the time derivatives (the derivatives had very large magnitudes), although at each iteration the conversion of the dipole parameters to spherical harmonic coefficients g_{nm} , h_{nm} and $\dot{g}_{nm}$, $\dot{h}_{nm}$ by equation (4) showed close agreement with a standard spherical harmonic model to degree and order 13 in the constant terms and degree and order 7 in the first derivative terms based on the same data set. The observability of the time variation of the individual dipoles over the short time period was poor, while the information content to the extent of determining the global time variation to degree 7 in spherical harmonics was strong. A priori values for the geocentric dipole derivatives were obtained from $\dot{g}_{10}$, $\dot{g}_{11}$ and $\dot{h}_{11}$ of the standard spherical harmonic model and the solution was then statistically constrained for the geocentric dipole using these values. The convergence using this technique showed much improvement.

To improve the observability of the time variation, observatory annual means data for a selected set of magnetic observatories from 1974-1977 was added to the above MAGSAT data set, and an unconstrained epoch 1980 dipole solution of 21° resolution (with a geocentric dipole) was obtained solving simultaneously for the observatory anomaly vectors (Langel et al, 1982). This solution is referred to as the 1974-1980 Dipole Model. The solution converged in three iterations, showing small correlations among the constant and derivative parameters (typically on the order of .01), although a few correlations reached values of approximately .4 between some nearest neighbor dipole parameters. The derivatives were on the order of one to two orders of magnitude smaller than the constant dipole parameters, with standard errors on the same order as the derivatives. This correlation structure is in stark

contrast to that observed in standard spherical harmonic models based on the same data set where the constant and derivative terms for a given degree and order may show correlations as high as .99. The dipole magnetization values per unit volume and their derivatives are given in Table III. With the exception of the geocentric dipole, all dipoles were placed at a geocentric radius of 3000 km. The volume associated with each dipole was that of a spherical shell of 40 km, thickness,

$$\text{Volume} = \left(21^\circ \times \frac{\pi}{180^\circ} \times 3000 \text{ km}\right)^2 \times 40 \text{ km} .$$

The same volume was arbitrarily assigned to the geocentric dipole. The observatory anomaly bias vectors are presented in Table IV, while the coefficients of the spherical harmonic expansion of the 93 dipoles through degree and order 24 (as calculated from equation (4) using magnetic moments given by dipole magnetizations multiplied by their respective volumes) are given in Table V.

The 1974-1980 Dipole Model is compared with candidate models for the 1975 IGRF presented by NASA, USGS and IGS in Tables VI through VIII. Table VI evaluates the fit to selected observatory annual means (Langel and Estes, 1982b) using the statistic $\bar{\sigma}$ defined by Langel et al. (1982), while Table VII compares the models using MAGSAT data. The dipole model performs well with respect to the candidate IGRF models. Table VIII displays the low degree and order spherical harmonic coefficients of the Dipole Model and the USGS candidate IGRF Secular Variation model, which is based on conventional techniques using more recent observatory annual means. The trends in the coefficients are very similar, although the magnitudes of the first degree dipole model terms are larger by a few nT than the USGS model. This is a result of the dipole model heavily utilizing Magsat data at epoch 1980. Field models based only on Magsat data yield $\dot{g}_{10}$ on the order of 28 nT/yr and $\dot{h}_{11}$ on the order of -20 nT/yr. The availability of ample observatory annual means data for years later than 1980 are required to more fully evaluate the different secular variation terms.

4.0 CONCLUSIONS

The modeling of the main field with an equivalent dipole representation has been found to be comparable to the standard spherical harmonic approach in accuracy. The 32° dipole density (42 dipoles) corresponds approximately to an eleventh degree/order spherical harmonic expansion (143 parameters) while the 21° dipole density (92 dipoles) corresponds to approximately a seventeenth degree and order expansion (288 parameters). Comparison of the number of arithmetic operations (multiplications, additions and trigonometric and square root evaluations) required to evaluate the magnetic field from dipole models and spherical harmonic models shows the dipole models to be superior in computational efficiency for spatial resolution better than 21° when three degrees-of-freedom unconstrained dipoles are utilized. The computational burden of field model evaluation is comparable to the standard spherical harmonic approach when the dipoles are constrained radially. Fixing of the dipole positions results in rapid convergence of the dipole solutions for single-epoch models. For time dependent models, a sufficiently long time interval of data or a priori values and statistics must be available for the derivatives to achieve convergence. In contrast to standard spherical harmonic models based on the same data, the correlation structure of dipole magnetic moment derivatives with the constant magnetic moment parameters is small, indicating the ability to strongly separate the constant field and the secular variation. The dipole model of 21° spatial resolution using observatory annual means data from 1974-1977 together with MAGSAT data performs very well when compared to candidate IGRF models of the main field and its secular variation based on conventional spherical harmonic techniques.

The dipole equivalent source approach for the main field was found not to be effective as a technique for distinquishing core and crustal fields. The investigation of possible indications of core fluid motions available from the equivalent source dipole model is left for further study.

Acknowledgements

This work was supported by NASA Contract NAS 5-26047. R. A. Langel supplied the global equivalent source crustal anomaly model.

5.0 REFERENCES

Alldredge, L. R., and L. Hurwitz, Radial dipoles as the sources of the Earth's main magnetic field. J. Geoph. Res. 69, 2631-2640, 1964.

Alldredge, L. R., and C. O. Stearns, Dipole model of the sources of the Earth's magnetic field and secular change. J. Geoph. Res. 74, 6583-6593, 1969.

Chapman, S. and J. Bartels, Geomagnetism. vol. 2, Oxford at Clarendon Press, London, 621 pp, 1940.

Dampney, C. N. G., The equivalent source technique. Geophysics 34, 39-53, 1969.

Hurwitz, L., Eccentric dipoles and spherical harmonic analysis, J. Geoph. Res. 65, 2555-2556, 1960.

Langel, R. A. and R. H. Estes, A geomagnetic field spectrum, J. Geoph. Res. Letters 9, 250-253, 1982a.

Langel, R. A. and R. H. Estes, A comparison of IGRF candidate models. Submitted to J. Geomag. Geoelectr., 1982b.

Langel, R. A., R. H. Estes, G. D. Mead, E. B. Fabiano and E. R. Lancaster, Initial geomagnetic field model from Magsat vector data, Geophy. Res. Let., 7, 793-796, 1980.

Langel, R. A., R. H. Estes and G. D. Mead, Some new methods in geomagnetic field modeling applied to the 1960-1980 epoch. Submitted to J. Geomag. Geoelectr., 1982.

Lowes, F. J. and S. K. Runcorn, The analysis of the geomagnetic secular variation. Phil Trans. Roy. Astron. Soc. London, A., 243, 525-546, 1951.

Mayhew, M. A., A computer program for reduction of Pogo satellite magnetic anomaly data to common elevation and to the pole. Interim report, NASA Contract S-41624-B, BTS, Inc., 1978.

Mayhew, M. A., Inversion of satellite magnetic anomaly data. J. Geoph. 45, 119-128, 1979.

Mayhew, M. A. and R. H. Estes, Constrained inversion of satellite magnetic anomaly data. Final Report, NASA/Goddard Space Flight Center Contract NAS 5-25698, Volume 3, 68 pp., 1981.

McNish, A. G., Physical representations of the geomagnetic field, Trans. Am. Geoph. Union 21, 287-291, 1940.

Stearns, C. O. and L. R. Alldredge, Models of sources of the Earth's magnetic field. in Methods of Computational Physics, 13, 61-92, 1973.

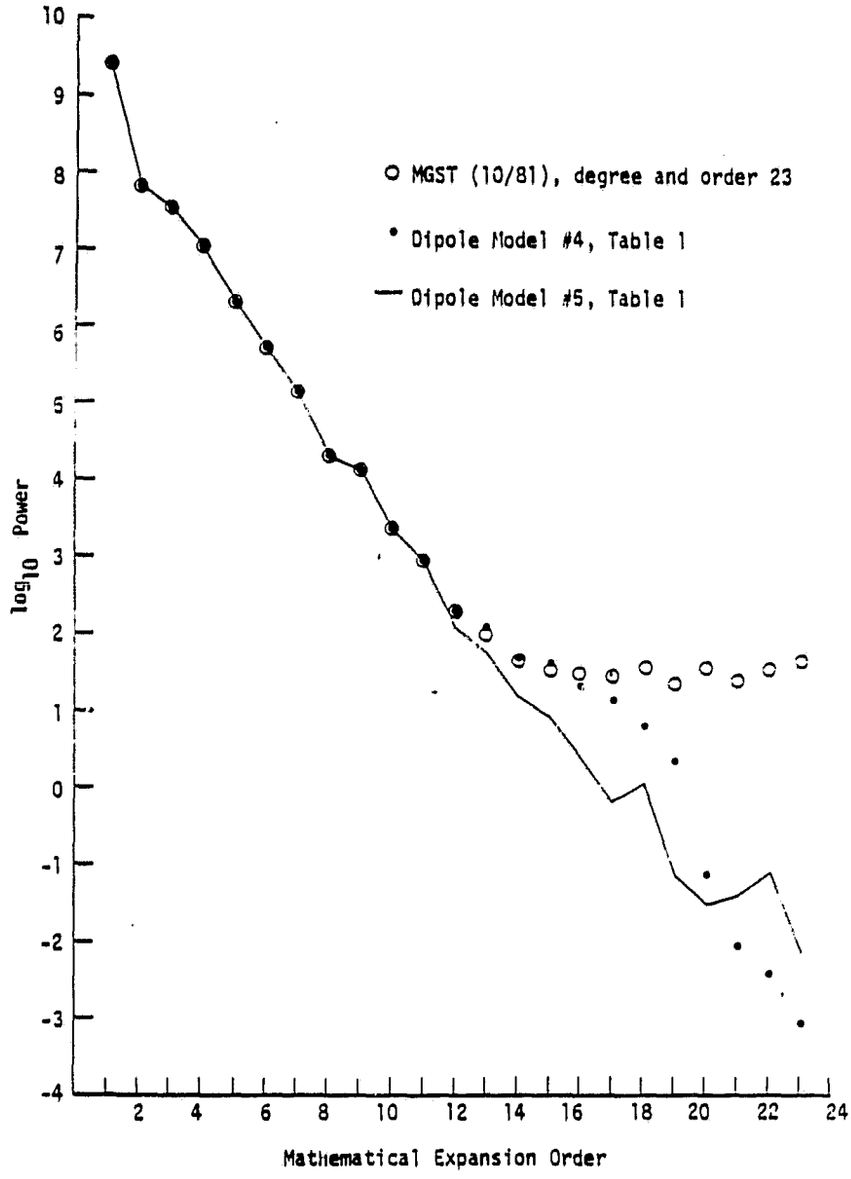

FIGURE 1 Power spectrum S_n of field model MGST (10/81) compared with spectra of Dipole Models 4 and 5

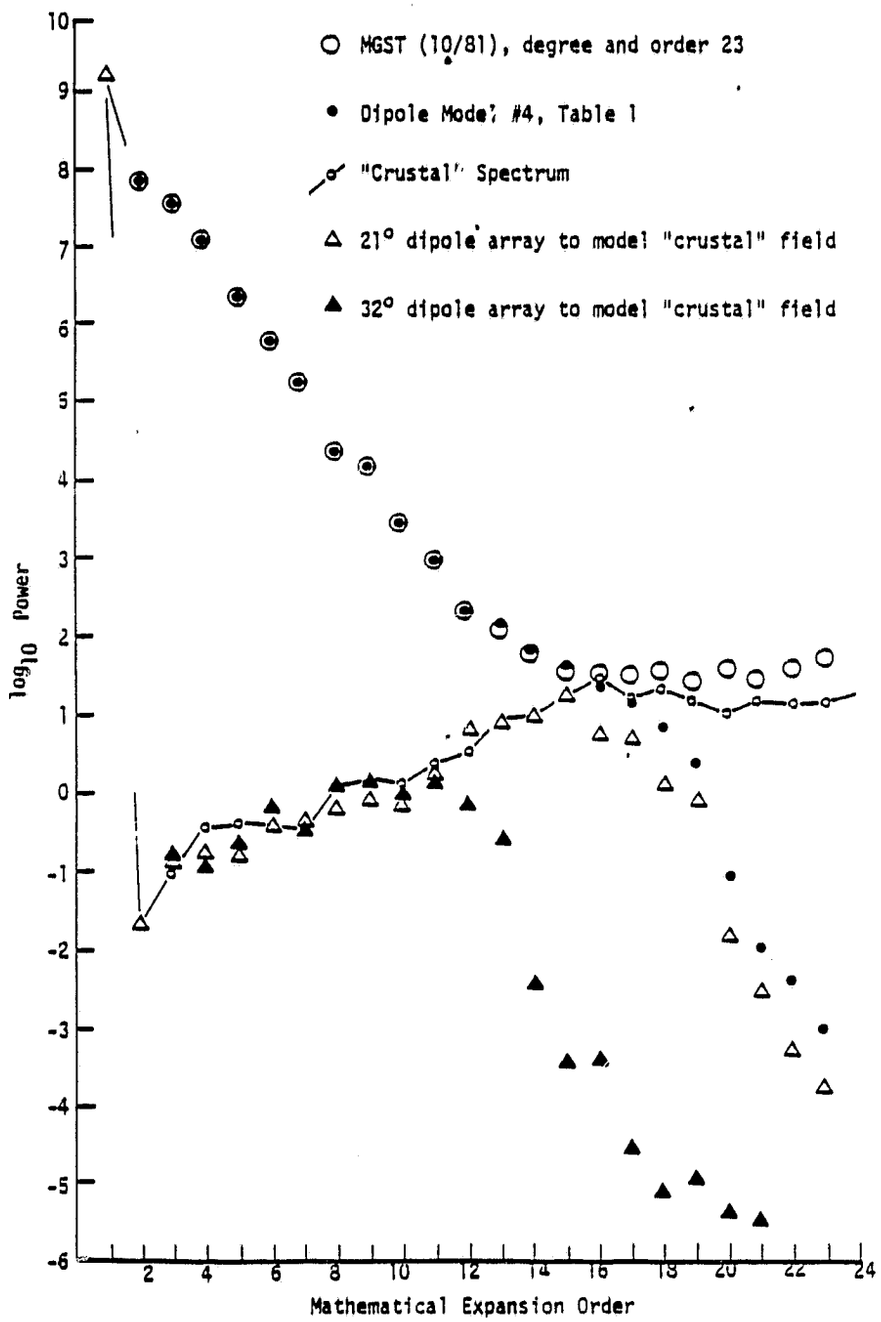

FIGURE 2 Power spectra S_n of synthetic "crustal" field and two dipole array models fit to this field compared with spectra of field model MGST (10/81) and Dipole Model 4

Table 1

Model #	Dipole Density at core/mantle boundary	# dipoles	(constrained/ unconstrained) # degrees of freedom	Geocentric Dipole included	External field	RMS to Nov. 5, 6 MAGSAT data
1	32°x32°	42	126	NO	YES	33γ
2	32°x32°	43	129	YES	YES	20γ
3	21°x21°	92	276	NO	YES	7γ
4	21°x21°	93	279	YES	YES	7γ
5	16°x16°	162	162	NO	YES	7γ

TABLE II

Simulation with POGO Crustal Anomaly Field Model

Synthesized Data Set is the Vector Sum of a Centered Dipole and the Crustal Field

Model	Dipole Density at core/mantle Boundary	# dipoles	# degrees of freedom	Geocentric Dipole included	Noise	RMS to synthesized data
6	--	1	3	YES	NO	8γ
7	32°x32°	43	129	YES	NO	2γ
8	32°x32°	43	129	YES	6γ	6γ
9	21°x21°	93	279	YES	NO	1γ
10	21°x21°	93	279	YES	6γ	6γ

TABLE III DIPOLE MAGNETIZATION VALUES PER UNIT VOLUME FOR 1974-1980 DIPOLE MODEL

	Lat	Lon	M_r	M_θ	M_ϕ	$\dot{M}_r$	$\dot{M}_\theta$	$\dot{M}_\phi$
1	89.	0.	636391.	783197.	5176538.	-81352.	-597.	-143046.
2	89.	0.	162147.	-1366251.	-767714.	-15920.	107319.	-41533.
3	27.	72.	-1736172.	2692943.	8288854.	-74720.	-55309.	-147190.
4	27.	144.	-1182209.	3303977.	-5192756.	-104435.	-66501.	138.
5	27.	216.	908838.	2244771.	-6869804.	-1979.	-51843.	125436.
6	27.	288.	844722.	-3257022.	-4569078.	3186.	30147.	-31909.
7	-27.	36.	-723747.	1946307.	2324348.	-247023.	74113.	75627.
8	-27.	108.	-460879.	1492084.	9570780.	34153.	91620.	78624.
9	-27.	180.	-402394.	817359.	9378499.	-108517.	-773.	81437.
10	-27.	252.	420177.	1931805.	17412110.	47935.	-606.	-189584.
11	-27.	324.	1551406.	-2405415.	1213328.	-82195.	-37191.	94895.
12	-89.	180.	33385.	-1734195.	1933453.	-125541.	193840.	-106740.
13	89.	0.	-113150.	-492280.	-12302224.	-118201.	888698.	599221.
14	69.	72.	-1796266.	4301414.	-3215917.	-22907.	462881.	-61520.
15	69.	144.	-987503.	1538964.	2888229.	22366.	22388.	-89745.
16	69.	216.	223154.	-1486442.	-1546419.	-40181.	-25400.	13679.
17	69.	288.	1749950.	-5301062.	-3079427.	-30682.	-143078.	148640.
18	49.	0.	-568137.	-1455547.	-14001755.	-6822.	9542.	11026.
19	53.	36.	-1706702.	4911116.	-2321654.	-29886.	186.	-62405.
20	49.	72.	-2810396.	1911957.	-1920555.	-13099.	52954.	21165.
21	53.	108.	-2898442.	1028184.	-1645051.	-6670.	-101715.	45343.
22	49.	144.	-1078357.	2210267.	-1389996.	-2775.	120390.	135559.
23	53.	180.	2021222.	1743116.	-2419949.	61757.	-104630.	55198.
24	49.	216.	828521.	581844.	-2753655.	71331.	105363.	-119065.
25	53.	252.	674195.	2771540.	-1816648.	142759.	-39045.	-34558.
26	49.	288.	-398894.	-2948298.	-765608.	131231.	84276.	-5333.
27	53.	324.	563614.	-1035880.	-2090776.	-33502.	-20866.	121802.
28	31.	24.	-1220552.	786395.	247945.	-59765.	25380.	85475.
29	31.	48.	-1593468.	-640869.	-76371.	-73951.	2119.	5622.
30	31.	96.	-3071616.	1466265.	-1733019.	137615.	-25913.	44756.
31	31.	120.	-3230677.	1045808.	-2472811.	76415.	11702.	-40808.
32	31.	168.	-960372.	1465551.	-833178.	-61141.	167361.	-19103.
33	31.	192.	-2954462.	-1879813.	-6020768.	-83165.	125280.	-124354.
34	31.	240.	1022276.	1853060.	-7514354.	-55669.	38797.	-62944.
35	31.	264.	728630.	1104366.	-6669935.	41117.	72646.	-38845.
36	31.	312.	1062696.	815209.	-2578599.	56758.	-41181.	-18354.
37	31.	336.	133093.	-785377.	-2992433.	-60426.	-81379.	29182.
38	9.	12.	565803.	1617396.	-1199634.	-52120.	-207431.	-52286.
39	11.	36.	965381.	2324851.	-2955951.	29762.	51303.	-51302.
40	9.	60.	-377749.	1156717.	-3186677.	-7974.	-126247.	140297.
41	11.	84.	-1092025.	4611826.	-2575344.	17363.	90755.	20632.
42	11.	108.	-823891.	547892.	-4165404.	-82526.	45282.	-78107.
43	9.	132.	-828846.	3329232.	-2591955.	32186.	-13864.	197227.
44	9.	156.	-1052682.	889345.	347769.	-83593.	22399.	-184835.
45	11.	180.	-1964761.	-1499157.	-524794.	-56345.	-255866.	88394.
46	9.	204.	-1087771.	1978276.	-1345452.	-21940.	23944.	69989.
47	9.	228.	399039.	1590399.	552127.	-51115.	9849.	-142959.
48	11.	252.	830796.	2750417.	258919.	13296.	-40770.	-135792.
49	9.	276.	603238.	486624.	3696652.	-32260.	27456.	201481.
50	9.	300.	639908.	-1883632.	-2407774.	-56721.	34710.	42154.
51	11.	324.	342356.	-264444.	-840790.	150344.	-60357.	27887.
52	9.	348.	984015.	-1361051.	-2884420.	-57716.	54333.	205e3.
53	-9.	24.	3341384.	3386406.	1099856.	33549.	86756.	35210.
54	-9.	48.	1678283.	2315477.	-587401.	32891.	58807.	-64346.
55	-11.	72.	829225.	893719.	-703642.	18784.	25580.	-3191.
56	-9.	96.	477620.	2439857.	1247433.	-138893.	-42470.	-5299.
57	-9.	120.	-1189908.	1534767.	390081.	127069.	-109532.	-246384.
58	-11.	144.	-782292.	857595.	1451206.	75681.	58930.	92108.
59	-9.	168.	-584399.	917978.	1772929.	147019.	-3410.	126770.
60	-9.	192.	-754738.	1574867.	-79520.	-68140.	63817.	-167579.
61	-11.	216.	574875.	142401.	851560.	90836.	3558.	-73085.
62	-9.	240.	739752.	1465745.	1803037.	-40571.	2000.	224357.
63	-9.	264.	1111960.	1156128.	1262872.	-55962.	-75404.	-8d74.
64	-11.	288.	221906.	1301478.	1121609.	-123345.	-33832.	-267469.
65	-9.	312.	1314459.	-688775.	-685221.	192830.	-25679.	-43030.
66	-9.	336.	1832986.	-4416455.	464560.	-1699.	59793.	116455.
67	-11.	0.	1664156.	-3305979.	-406169.	26112.	25749.	63195.
68	-11.	60.	-752727.	1979682.	5448324.	-1658.	-31332.	-155481.
69	-11.	84.	-852216.	229181.	3339347.	12278.	-30532.	12802.
70	-11.	132.	140844.	-971031.	808310.	-26597.	-22742.	130144.
71	-11.	156.	112078.	-1271917.	1257765.	-113312.	192406.	-140721.
72	-11.	204.	593592.	-274343.	1056937.	-7428.	-19785.	67593.
73	-11.	228.	617060.	340976.	987907.	-83670.	-42016.	5466.
74	-11.	276.	794157.	189012.	921374.	71473.	73707.	197522.
75	-11.	300.	250657.	5040054.	1608079.	75686.	-24602.	-97579.
76	-11.	348.	1593202.	-1182588.	579154.	-80669.	68148.	-239032.
77	-11.	12.	1043967.	-2274983.	156279.	14224.	-182819.	104476.
78	-11.	36.	-777629.	1435336.	1527445.	63682.	-21725.	-36816.
79	-11.	36.	-224667.	2330228.	2119927.	140744.	-25378.	103466.
80	-11.	108.	782153.	1437956.	753464.	-57628.	-80534.	-57838.
81	-11.	144.	557913.	2139160.	363766.	-58779.	89998.	14586.
82	-11.	180.	-187140.	-1088950.	34612.	-23196.	-303065.	-123031.
83	-11.	216.	692937.	464420.	809002.	100225.	161855.	-37952.
84	-11.	252.	991561.	1397292.	117172.	-8349.	-81910.	-42259.
85	-11.	288.	-640817.	1262211.	712603.	-34910.	57623.	72993.
86	-11.	324.	763591.	-1913546.	2003480.	10633.	50593.	152809.
87	-11.	0.	881524.	-1710324.	1746957.	29812.	-87561.	37866.
88	-89.	36.	-437550.	2158605.	145120.	77905.	82912.	-119561.
89	-89.	108.	1470384.	939920.	4165891.	-67795.	320399.	169076.
90	-89.	180.	10821131.	-2206310.	1991113.	76983.	107740.	525775.
91	-89.	252.	908268.	1829628.	-1056054.	-101875.	-23845.	-395958.
92	-89.	324.	1116849.	391093.	806462.	-60594.	70777.	-251283.
93	0.	0.	-27511.	99267760.	21933987.	27064.	-47460.	-31842.

TABLE IV OBSERVATORY ANOMALY BIASES FROM 1974-1980
DIPOLE MODEL SOLUTION (nT)

	Observatory	Lat	Lon	Alt	B_x	B_y	B_z
1	ALERT	82.50	-62.50	0.06	83.5	50.5	-328.0
2	ALMA ATA	43.25	76.92	1.30	146.2	-1.2	-224.0
3	ALMERIA	36.85	-2.46	0.06	2.5	-24.3	-1.0
4	AMBERLEY	-43.15	172.72	0.04	20.2	-30.5	96.0
5	ANNAMALAINAGAR	11.37	79.68	0.0	166.6	-201.6	-184.0
6	APIA	-13.81	-171.78	0.0	13.6	109.8	-921.7
7	AQUILA	42.38	13.32	0.63	42.9	33.9	-11.4
8	BAKER STREET	64.33	-96.03	0.04	158.5	-50.5	0.1
9	BANG BIG	4.44	18.56	0.44	-348.0	-70.6	326.3
10	BARROW	71.30	-156.75	0.0	29.7	-70.8	12.4
11	BELSK	51.84	20.79	0.18	133.6	132.9	320.5
12	BEREZNAYKI	49.82	73.08	0.0	-368.4	-25.2	277.7
13	BOULDER	40.14	-105.24	1.65	2.6	54.0	-161.8
14	CASTLE ROCK	37.44	-122.13	0.46	-82.1	-11.7	-7.2
15	CHA PA	22.35	103.83	1.55	-259.0	1.0	-392.2
16	CHAMBON FORET	48.02	2.26	0.15	-44.2	-31.5	114.5
17	CHELYUSKIN	77.72	104.28	0.01	6.6	-79.1	90.0
18	COIMBRA	40.22	-8.42	0.10	13.4	-40.3	15.7
19	COLLEGE	64.86	-147.84	0.09	33.7	-34.8	-80.6
20	DALLAS	32.99	-96.75	0.21	-11.0	13.8	-90.3
21	DIKSON	73.55	80.57	0.02	-32.0	-141.0	-154.3
22	DOMBAS	62.07	9.12	0.66	-78.4	-71.7	-190.6
23	DOURBES	50.10	4.59	0.23	32.9	-16.1	36.2
24	DUMONT DURV	-66.66	140.01	0.04	-36.6	-476.2	-3023.6
25	DUSHETI	42.09	44.70	0.98	-210.4	-4.3	-129.8
26	DYMER	50.72	30.30	0.18	11.4	66.4	104.2
27	FORT CHURCHILL	58.77	-94.10	0.04	-111.6	68.4	-137.8
28	FREDERICKSBURG	38.21	-77.37	0.07	79.4	-56.4	80.2
29	FUQUENE	5.47	-73.74	2.54	83.6	-50.7	8.2
30	FURSTENFELDBRUCK	48.17	11.28	0.57	14.7	-12.8	18.4
31	GNANGARA	-31.78	115.95	0.06	-13.2	-125.5	354.0
32	GORNOTAYEZHNAYA	43.68	132.17	0.30	5.9	10.9	-93.9
33	GREAT WHALE R	55.27	-77.78	0.02	312.9	109.8	-92.5
34	GROCKA	44.63	20.77	0.23	1.5	-54.4	-62.3
35	GUAM	13.58	144.87	0.04	83.3	72.3	62.5
36	HARTLAND	51.00	-4.48	0.09	-19.9	10.0	65.[illegible]
37	HERMANUS	-34.42	19.22	0.03	53.8	-7.8	19.[illegible]
38	HONOLULU	21.32	-158.00	0.0	-187.8	118.9	-321.4
39	HUANCAYO	-12.04	-75.34	3.31	77.2	54.1	27.3
40	HYDERABAD	17.41	78.55	0.50	302.5	-12.3	413.1
41	ISTANBL KNDILLI	41.06	29.06	0.13	229.6	129.5	-22.9
42	KAKIOKA	36.23	140.19	0.03	-68.1	17.9	-130.1
43	KERGUELEN	-49.35	70.20	0.05	248.9	183.5	564.0
44	KLYUCHI	55.03	82.90	0.0	230.2	-106.1	-30.2
45	KRASNAYA PAKHRA	55.48	37.31	0.20	169.9	-32.9	208.0
46	LEIRVOGUR	64.18	-21.70	0.01	-325.9	620.2	-477.4
47	LERWICK	60.13	-1.18	0.08	-113.7	181.3	82.1
48	LOGRONO	42.46	-2.51	0.44	28.4	-13.4	39.2
49	LOPARSKOYE	68.25	33.08	0.21	123.5	342.7	-477.9
50	LOVO	59.35	17.83	0.02	69.3	-14.4	42.2
51	LUANDA BELAS	-8.92	13.17	0.05	283.1	-62.4	334.7
52	LUNPING	25.00	121.17	0.10	-245.9	165.7	4.5
53	LVOV	49.90	23.75	0.33	167.0	100.0	155.8
54	MACQUARIE ISLND	-54.50	158.95	0.0	325.4	-19.1	293.1
55	MAWSON	-67.60	62.88	0.0	90.9	39.9	197.4
56	MEANOOK	54.62	-113.33	0.68	110.5	20.0	-115.6
57	MEMAMBETSU	43.91	144.19	0.04	-247.7	140.0	21.5
58	MIRNYY	-66.55	93.02	0.02	-39.7	69.3	-467.1
59	MOLODEZHNAYA	-67.67	45.85	0.0	43.0	-35.1	-241.2
60	MOULD BAY	76.20	-119.40	0.15	-54.0	-36.8	-51.2
61	NAIROBI	-1.33	36.81	1.67	-5.8	68.8	-70.1
62	NEWPORT	48.26	-117.12	0.78	-22.4	126.2	-98.7
63	NIEMEGK	52.07	12.67	0.08	0.4	-4.4	-54.3
64	NOVOLAZAREVSKAY	-70.77	11.83	0.0	-268.8	130.1	33.9
65	NURMIJARVI	60.51	24.65	0.11	310.3	-116.9	133.4
66	OTTAWA	45.40	-75.55	0.[illegible]	212.8	-139.2	153.0
67	PANAGYURISHTE	42.52	24.18	0.56	-152.7	-172.5	-195.1
68	PARAMARIBO	5.81	-55.22	0.08	38.9	-140.0	-174.3
69	PARATUNKA	52.90	158.43	0.11	-329.6	245.6	231.7
70	PATRONY	52.17	104.45	0.54	74.8	53.1	-115.9
71	PILAR	-31.67	-63.83	0.34	23.6	228.8	-258.9
72	PLAISANCE	-20.43	57.67	0.0	0.0	0.0	791.6
73	PLESHENITZI	54.50	27.88	0.20	313.2	123.7	-125.8
74	PODKAM TUNGUSKA	61.60	90.00	0.0	107.1	43.8	-303.0
75	PORT MORESBY	-9.41	147.15	0.08	-74.6	47.4	246.0
76	QUETTA	30.19	66.95	1.75	-54.6	72.0	-101.2
77	QUIACA	-22.10	-65.61	3.45	91.8	98.9	-84.9
78	RESOLUTE BAY	74.70	-94.90	0.02	-36.0	-6.1	51.1
79	RUDE SKOV	55.84	12.46	0.05	59.9	-13.1	-7.1
80	SAN JUAN	18.12	-66.15	0.40	-55.6	186.6	183.1
81	SAN MIGUEL	37.77	-25.65	0.18	681.9	560.2	1739.8
82	SANAE	-70.30	-2.37	0.05	-46.1	-4.4	-130.7
83	SCOTT BASE	-77.85	166.78	0.0	-2301.7	-919.8	-3925.4
84	SHIMOSATO	33.58	135.93	0.06	-155.3	68.2	-28.2
85	SITKA	57.06	-135.33	0.02	30.1	19.5	-69.9
86	SODANKYLA	67.37	26.63	0.18	-140.3	-100.0	-544.1
87	ST JOHN S	47.59	-52.68	0.0	111.1	22.2	60.6
88	STEKOLNIY	60.12	151.02	0.0	-228.1	-739.3	44.1
89	STEPANOVKA	46.78	30.88	0.14	-92.3	-711.7	53.8
90	TANANARIVE	-18.92	47.50	1.38	344.9	2.2	-402.5
91	TENERIFE	28.48	-16.28	0.31	-468.3	80.3	-947.3
92	TEOLOYU X	19.75	-99.18	2.28	0.3	81.9	-58.3
93	TIHANY	46.90	17.89	0.19	34.3	-20.8	-45.7
94	TIKSI 2	71.58	129.00	0.04	-8.9	-142.7	-8.3
95	TOOLANGI	-37.53	145.47	0.46	30.7	-86.7	60.7
96	TRIVANDRUM	8.48	76.95	0.30	160.5	113.5	50.4
97	TSUMEB	-19.22	17.70	0.0	30.7	-106.8	96.3
98	TUCSON	32.25	-110.83	0.77	-57.3	-55.1	116.9
99	UELEN	66.16	-169.84	0.01	-7.3	44.4	-83.6
100	ULAN BATOR	47.85	107.05	0.0	64.0	21.5	-181.5
101	VALENTIA	51.93	-10.25	0.01	153.1	-52.4	25.7
102	VANNOVSKAYA	37.95	58.11	0.57	164.5	102.0	15.2
103	VICTORIA	48.52	-123.42	0.18	35.5	24.0	-302.3
104	VOSTOK	-78.45	106.87	3.50	64.2	71.6	-70.3
105	VOYEYKOVO	59.95	30.70	0.07	119.6	9.3	-249.3
106	VYSOKAY BRAVO	56.73	61.07	0.29	-229.3	-128.2	-490.5
107	WINGST	53.74	9.07	0.05	86.8	41.3	-34.7
108	YAKUTSK	62.02	129.72	0.10	118.6	-1174.5	107.4
109	YANGI-BAZAR	41.33	69.62	0.81	-304.4	34.2	-147.9
110	YUZHNO SAKHA	46.95	142.72	0.07	-76.3	-53.7	57.4

ORIGINAL PAGE IS OF POOR QUALITY

TABLE V SPHERICAL HARMONIC EXPANSION COEFFICIENTS OF 1974-1980 DIPOLE MODEL (nT)

n	m	g_{nm}	h_{nm}	$\dot{g}_{nm}$	$\dot{h}_{nm}$
1	0	-29987.00	0.0	25.43	0.0
1	1	-1956.83	5604.02	13.48	-17.97
2	0	-1996.95	0.0	-18.30	0.0
2	1	3027.46	-2129.43	1.49	-8.66
2	2	1663.16	-200.19	5.72	-23.44
3	0	1280.53	0.0	-5.12	0.0
3	1	-2180.95	-334.39	-6.82	4.33
3	2	1251.25	271.50	-3.51	2.02
3	3	833.01	-252.13	-1.44	-8.02
4	0	937.80	0.0	-1.32	0.0
4	1	782.35	212.30	-2.42	1.67
4	2	397.32	-256.42	-6.07	0.55
4	3	-419.59	52.89	-0.63	2.78
4	4	197.85	-297.37	-5.96	-0.64
5	0	-217.44	0.0	0.32	0.0
5	1	357.46	45.72	-0.07	1.09
5	2	260.57	149.37	-1.01	1.20
5	3	-74.35	-150.56	-4.60	-0.43
5	4	-161.77	77.90	1.14	1.40
5	5	-48.13	92.17	0.52	2.05
6	0	48.42	0.0	1.33	0.0
6	1	65.14	-114.45	1.75	-0.29
6	2	42.10	93.26	2.82	-1.64
6	3	-192.01	70.71	2.55	0.50
6	4	3.51	-43.27	1.71	0.42
6	5	14.17	-2.18	-0.93	2.31
6	6	107.22	-17.04	-0.85	1.92
7	0	72.06	0.0	0.90	0.0
7	1	-59.29	-82.40	-1.16	-1.45
7	2	-1.68	-27.06	-0.42	0.14
7	3	20.74	-5.05	0.34	-1.05
7	4	-12.31	16.12	0.35	0.44
7	5	10.53	-17.89	-0.75	-0.38
7	6	-1.76	-23.01	-0.25	0.52
7	7	18.46	-9.81	-0.08	0.39
8	0	6.64	0.0	0.19	-0.0
8	1	-0.08	7.04	0.21	-0.25
8	2	-10.75	-17.57	1.67	0.13
8	3	-7.16	3.85	-0.39	0.06
8	4	4.38	-22.09	-1.06	-0.71
8	5	2.56	9.03	-0.73	-0.92
8	6	-5.99	16.16	1.01	-1.63
8	7	-1.43	-13.50	-0.52	0.25
8	8	5.33	-14.58	-0.44	1.01
9	0	10.46	0.0	-0.66	0.0
9	1	-1.46	-21.07	0.43	-0.02
9	2	-12.14	15.38	0.25	0.05
9	3	9.48	-8.92	0.04	-0.11
9	4	-3.49	-5.16	0.44	-0.21
9	5	-1.03	-6.58	0.65	0.55
9	6	6.97	9.07	-0.55	-0.03
9	7	-1.23	9.84	-0.69	-0.63
9	8	-5.13	-5.79	1.81	-0.11
9	9	-3.20	2.01	0.08	0.13
10	0	-3.75	0.0	0.08	0.0
10	1	2.16	-1.18	0.18	-1.22
10	2	-5.53	0.46	-1.07	-1.28
10	3	-1.86	2.89	-0.11	0.33
10	4	4.76	5.53	-0.29	0.20
10	5	3.51	-4.18	-0.09	-0.56
10	6	0.66	-0.34	-1.06	-0.46
10	7	2.18	-1.09	0.81	0.89
10	8	2.83	3.46	-0.67	1.22
10	9	0.26	-0.33	-0.09	-0.37
10	10	-4.83	-6.34	1.58	-0.79
11	0	2.53	0.0	0.42	0.0
11	1	-1.14	0.78	-0.54	-0.19
11	2	-1.50	1.79	-0.56	0.08
11	3	2.43	-1.15	-0.08	0.06
11	4	-0.26	-2.96	0.48	-0.38
11	5	-0.70	0.65	0.05	0.18
11	6	-0.56	-0.07	-0.13	-0.30
11	7	1.59	-2.36	-0.02	-0.33
11	8	1.56	-0.39	0.16	-0.66
11	9	-0.75	-1.59	-0.61	-0.47
11	10	1.92	-1.62	0.31	-0.20
11	11	3.61	1.23	-0.95	-0.17
12	0	-1.56	0.0	-0.26	0.0
12	1	-0.06	0.39	-0.31	-0.30
12	2	-0.30	0.76	0.44	-0.06
12	3	-0.09	2.20	-0.16	-0.32
12	4	0.58	-1.49	-0.20	0.32

n	m	g_{nm}	h_{nm}	$\dot{g}_{nm}$	$\dot{h}_{nm}$
12	5	-0.54	0.13	-0.66	-0.05
12	6	-0.45	0.17	-0.07	-0.25
12	7	-0.30	-0.23	-0.08	-0.31
12	8	-0.23	0.09	-0.17	-0.28
12	9	-0.42	-0.23	-0.05	-0.29
12	10	0.03	-1.35	-0.08	0.05
12	11	-0.75	0.69	0.62	-0.25
12	12	-0.56	0.98	0.02	0.22
13	0	-0.23	0.0	-0.04	0.0
13	1	-0.19	-0.65	0.06	-0.08
13	2	0.37	0.15	0.03	-0.01
13	3	-0.52	1.36	-0.12	-0.10
13	4	-0.01	-0.45	-0.10	-0.11
13	5	0.89	-0.65	-0.03	0.02
13	6	-0.36	-0.31	-0.14	-0.10
13	7	0.27	0.72	-0.05	0.05
13	8	-0.65	0.04	-0.11	-0.22
13	9	0.08	0.75	0.00	-0.00
13	10	-0.07	0.18	-0.01	-0.01
13	11	0.48	0.04	-0.08	-0.05
13	12	-0.62	-0.32	0.04	0.05
13	13	-0.24	-1.15	-0.14	0.10
14	0	-0.26	0.0	-0.02	0.0
14	1	0.29	0.28	-0.04	-0.01
14	2	0.02	-0.54	-0.03	0.02
14	3	-0.12	-0.02	-0.02	0.02
14	4	-0.21	0.20	-0.07	0.02
14	5	0.36	-0.01	-0.02	0.00
14	6	-0.07	0.33	0.04	0.02
14	7	-0.05	0.38	0.00	-0.01
14	8	-0.05	0.15	-0.03	-0.02
14	9	0.25	0.22	-0.03	0.06
14	10	-0.25	-0.47	-0.03	-0.01
14	11	-0.33	-0.11	-0.01	-0.04
14	12	-0.15	0.13	0.01	-0.02
14	13	0.54	0.05	-0.06	-0.00
14	14	0.98	0.12	-0.03	-0.02
15	0	0.26	0.0	0.00	0.0
15	1	-0.53	-0.24	0.02	0.01
15	2	-0.17	-0.12	0.00	0.00
15	3	0.58	0.05	-0.00	0.00
15	4	-0.25	0.11	-0.03	-0.00
15	5	-0.26	-0.37	-0.02	0.01
15	6	-0.18	0.08	-0.01	0.01
15	7	-0.19	-0.30	0.00	0.00
15	8	-0.11	-0.22	-0.01	0.00
15	9	-0.33	0.20	0.02	0.01
15	10	-0.22	-0.09	-0.01	-0.01
15	11	0.21	0.09	-0.01	-0.00
15	12	-0.28	-0.27	0.01	0.02
15	13	-0.40	-0.24	0.01	-0.01
15	14	0.29	0.70	-0.01	0.00
15	15	0.26	0.51	-0.02	-0.01
16	0	0.05	0.0	-0.01	0.0
16	1	-0.21	0.43	0.00	0.00
16	2	-0.12	0.20	-0.01	-0.00
16	3	-0.23	0.10	0.00	0.01
16	4	-0.09	-0.00	0.00	0.01
16	5	0.01	-0.19	0.01	0.00
16	6	-0.22	-0.13	-0.00	0.01
16	7	-0.04	-0.01	-0.00	-0.01
16	8	0.06	-0.05	-0.01	-0.01
16	9	-0.17	-0.02	-0.00	0.00
16	10	-0.07	-0.16	0.02	-0.00
16	11	-0.16	-0.22	0.00	-0.01
16	12	-0.03	-0.11	-0.01	0.00
16	13	0.18	-0.15	-0.01	0.01
16	14	-0.03	-0.23	-0.00	-0.00
16	15	-0.12	-0.05	-0.01	0.00
16	16	-0.12	0.06	-0.00	0.00
17	0	-0.10	0.0	-0.00	0.0
17	1	-0.15	-0.32	-0.00	-0.00
17	2	0.16	-0.18	-0.00	-0.00
17	3	0.06	0.13	-0.00	-0.00
17	4	-0.04	0.16	-0.00	-0.00
17	5	-0.06	-0.22	0.00	0.00
17	6	-0.08	-0.01	0.00	0.00
17	7	-0.05	0.01	0.00	0.00
17	8	0.05	0.07	0.00	-0.00
17	9	0.07	0.19	0.00	0.01
17	10	-0.05	-0.33	-0.00	0.00
17	11	-0.03	-0.06	-0.00	0.00
17	12	-0.10	-0.02	-0.00	-0.00

n	m	g_{nm}	h_{nm}	$\dot{g}_{nm}$	$\dot{h}_{nm}$
17	13	0.05	0.11	-0.00	0.00
17	14	0.26	0.33	-0.00	0.00
17	15	-0.03	-0.47	0.00	-0.00
17	16	-0.29	-0.14	-0.00	-0.00
17	17	0.05	-0.02	0.00	0.00
18	0	-0.03	0.0	-0.0	0.0
18	1	-0.04	0.18	-0.00	-0.00
18	2	-0.01	0.00	0.00	-0.00
18	3	-0.04	-0.03	-0.00	-0.00
18	4	-0.01	-0.07	0.00	0.00
18	5	-0.02	-0.01	-0.00	-0.00
18	6	0.00	0.03	0.00	0.00
18	7	-0.04	-0.00	-0.00	0.00
18	8	-0.03	-0.01	-0.00	-0.00
18	9	-0.04	-0.05	-0.00	-0.00
18	10	-0.04	-0.04	-0.00	0.00
18	11	-0.03	-0.01	-0.00	-0.00
18	12	-0.03	-0.02	0.00	0.00
18	13	-0.01	-0.01	-0.00	-0.00
18	14	0.05	-0.13	-0.00	0.00
18	15	0.02	-0.14	-0.00	-0.00
18	16	-0.07	-0.06	-0.00	0.00
18	17	0.00	-0.05	-0.00	0.00
18	18	-0.01	-0.01	-0.00	0.00
19	0	-0.05	0.0	-0.00	0.0
19	1	-0.01	0.01	0.00	0.00
19	2	-0.03	-0.03	0.00	-0.00
19	3	-0.03	-0.01	0.00	-0.00
19	4	-0.01	0.00	0.00	0.00
19	5	-0.04	-0.01	-0.00	-0.00
19	6	-0.02	0.01	-0.00	-0.00
19	7	-0.02	0.03	-0.00	-0.00
19	8	0.00	0.02	-0.00	0.00
19	9	0.00	-0.02	-0.00	-0.00
19	10	-0.03	-0.05	0.00	0.00
19	11	-0.03	0.00	0.00	0.00
19	12	0.02	0.03	-0.00	-0.00
19	13	0.01	-0.02	-0.00	0.00
19	14	-0.01	0.03	-0.00	-0.00
19	15	-0.06	-0.13	0.00	0.00
19	16	-0.01	-0.01	-0.00	-0.00
19	17	-0.01	0.02	-0.00	0.00
19	18	-0.01	-0.02	0.00	-0.00
19	19	-0.01	-0.00	0.00	0.00
20	0	-0.01	0.0	-0.00	0.0
20	1	0.02	-0.00	-0.00	-0.00
20	2	-0.01	0.00	-0.00	-0.00
20	3	-0.01	0.00	0.00	0.00
20	4	-0.00	0.01	-0.00	-0.00
20	5	0.01	-0.00	-0.00	-0.00
20	6	0.01	-0.01	0.00	0.00
20	7	0.01	-0.00	-0.00	-0.00
20	8	-0.00	0.01	0.00	0.00
20	9	0.00	-0.01	-0.00	-0.00
20	10	-0.00	-0.01	0.00	0.00
20	11	0.00	-0.01	0.00	-0.00
20	12	-0.01	-0.01	0.00	0.00
20	13	-0.01	0.00	0.00	0.00
20	14	-0.00	-0.01	0.00	-0.00
20	15	-0.01	-0.01	0.00	-0.00
20	16	-0.00	-0.00	0.00	-0.00
20	17	-0.00	0.00	-0.00	0.00
20	18	-0.00	0.01	-0.00	0.00
20	19	-0.01	-0.00	-0.00	-0.00
20	20	-0.00	-0.00	-0.00	-0.00
21	0	-0.01	0.0	-0.00	0.0
21	1	-0.01	0.00	0.00	0.00
21	2	-0.00	0.00	0.00	-0.00
21	3	0.00	-0.00	0.00	-0.00
21	4	0.00	-0.00	0.00	0.00
21	5	0.00	-0.00	-0.00	0.00
21	6	0.00	-0.01	-0.00	0.00
21	7	0.00	-0.00	-0.00	0.00
21	8	0.00	-0.00	-0.00	-0.00
21	9	-0.00	-0.01	-0.00	-0.00
21	10	-0.00	-0.00	-0.00	0.00
21	11	0.00	-0.00	-0.00	0.00
21	12	0.00	-0.00	0.00	0.00
21	13	-0.00	-0.00	-0.00	-0.00
21	14	-0.01	-0.01	0.00	0.00
21	15	-0.01	0.01	0.00	0.00
21	16	-0.01	0.00	-0.00	-0.00
21	17	0.00	0.00	-0.00	-0.00

n	m	g_{nm}	h_{nm}	$\dot{g}_{nm}$	$\dot{h}_{nm}$
21	18	-0.00	-0.00	0.00	-0.00
21	19	-0.00	0.00	0.00	-0.00
21	20	0.00	-0.01	-0.00	-0.00
21	21	0.00	-0.00	0.00	-0.00
22	0	0.00	0.0	-0.00	0.0
22	1	0.00	0.00	-0.00	-0.00
22	2	0.00	0.00	-0.00	0.00
22	3	0.00	-0.00	-0.00	-0.00
22	4	-0.00	0.00	0.00	0.00
22	5	0.00	0.00	-0.00	-0.00
22	6	0.00	-0.00	-0.00	0.00
22	7	0.00	-0.00	0.00	0.00
22	8	-0.00	-0.00	0.00	0.00
22	9	-0.00	-0.00	0.00	0.00
22	10	-0.00	0.00	-0.00	0.00
22	11	0.00	-0.00	0.00	-0.00
22	12	-0.00	0.00	0.00	0.00
22	13	-0.00	0.00	0.00	0.00
22	14	-0.00	-0.00	0.00	-0.00
22	15	0.00	0.00	0.00	-0.00
22	16	-0.00	0.00	-0.00	0.00
22	17	-0.00	-0.00	-0.00	-0.00
22	18	-0.00	0.00	0.00	-0.00
22	19	0.00	-0.00	-0.00	0.00
22	20	-0.00	-0.00	-0.00	0.00
22	21	-0.00	0.00	0.00	-0.00
22	22	0.00	0.00	0.00	0.00
23	0	-0.00	0.0	0.00	0.0
23	1	0.00	0.00	0.00	-0.00
23	2	-0.00	0.00	0.00	-0.00
23	3	-0.00	0.00	-0.00	0.00
23	4	-0.00	0.00	0.00	0.00
23	5	0.00	-0.00	-0.00	-0.00
23	6	-0.00	-0.00	0.00	-0.00
23	7	0.00	0.00	-0.00	-0.00
23	8	-0.00	-0.00	-0.00	0.00
23	9	0.00	0.00	-0.00	-0.00
23	10	-0.00	-0.00	-0.00	0.00
23	11	0.00	-0.00	0.00	0.00
23	12	0.00	-0.00	0.00	0.00
23	13	0.00	-0.00	0.00	0.00
23	14	-0.00	0.00	0.00	0.00
23	15	-0.00	0.00	-0.00	0.00
23	16	0.00	-0.00	0.00	0.00
23	17	-0.00	-0.00	-0.00	0.00
23	18	-0.00	-0.00	-0.00	0.00
23	19	-0.00	0.00	0.00	-0.00
23	20	-0.00	-0.00	0.00	-0.00
23	21	-0.00	0.00	-0.00	-0.00
23	22	0.00	0.00	-0.00	-0.00
23	23	0.00	-0.00	-0.00	-0.00
-1	-1	0.0	0.0	0.0	0.0

TABLE VI $\overline{\sigma}$ OF CANDIDATE IGRF MODELS AND 1974-1980 DIPOLE MODEL (nT)

	YEAR:	1975	1976	1978	1979
$\overline{\sigma}_x$					
	NASA	125			
	USGS	130	125	145	115
	IGS	155			
	DIPOLE	140	120	130	120
$\overline{\sigma}_y$					
	NASA	100			
	USGS	100	90	100	95
	IGS	110			
	DIPOLE	110	90	110	85
$\overline{\sigma}_z$					
	NASA	175			
	USGS	195	175	155	140
	IGS	190			
	DIPOLE	180	165	170	150

TABLE VII STATISTICAL COMPARISON OF CANDIDATE IGRF MODELS AND 1974-1980 DIPOLE MODEL ON SELECTED MAGSAT DATA (nT) AT EPOCH 1980

	Spherical Harmonic Expansion Order	σ_B	σ_X	σ_Y	σ_Z
NASA	(10)	13.3	11.3	11.2	14.9
USGS	(10)	15.7	10.3	10.2	13.0
IGS	(10)	112.0	85.2	66.9	118.0
DIPOLE	(16)	7.0	6.8	8.0	8.6
DIPOLE	(10)	11.2	10.0	10.2	12.4

Table VIII

Low degree and order spherical harmonic coefficients at Epoch 1980 derived from EQUIVALENT DIPOLE MODEL of 21° resolution using MAGSAT data and observatory Annual Means from 1974-1977.

		Dipole Model				USGS IGRF Candidate Model Epoch 1980	
Degree	Order	g_{nm}	h_{nm}	$\dot{g}_{nm}$	$\dot{h}_{nm}$	$\dot{g}_{nm}$	$\dot{h}_{nm}$
1	0	-29987.0		25.4		21.7	
1	1	-1986.8	5604.0	13.5	-17.9	11.0	-14.4
2	0	-1996.9		-18.3		-18.8	
2	1	3027.5	-2129.4	1.5	-8.7	3.3	-12.6
2	2	1663.2	-200.2	5.7	-23.4	4.3	-26.3
3	0	1280.5		-5.1		0.2	
3	1	-2180.9	-334.4	-6.8	4.3	-7.1	1.4
3	2	1251.3	271.5	-3.5	2.0	-1.4	2.6
3	3	833.0	-252.1	-1.4	-8.0	-0.1	-7.6
4	0	937.8		-1.3		-1.2	
4	1	782.3	212.3	-2.4	1.7	-0.9	4.9
4	2	397.3	-256.4	-6.1	0.5	-6.9	2.2
4	3	-419.6	52.9	-0.6	2.8	-1.6	4.4
4	4	197.8	-297.4	-5.9	-0.6	-3.0	-0.4

APPENDIX
SOFTWARE DESCRIPTION AND FLOW CHART

The software system was developed to recover a multiple dipole representation of the main field and is coded in FORTRAN. An assembly language subroutine is utilized to obtain required computer core memory dynamically in the IBM 360 and 3081 environment. The analysis utilizes an iterative least squares algorithm with the capability for a priori information. The dipoles are set by user input to a specified radius within the earth, and are centered on equal area blocks. The system has the option to solve for either the dipole magnitudes only (with the dipole orientations constrained to a preselected direction), or to allow full freedom of orientation for the dipoles and solve for the three components.

The least squares equations are as follows:

$$\delta\hat{X}_{n+1} = (A^T W A + \Lambda_o^{-1})^{-1} \left[A^T W \delta y_n + \Lambda_o^{-1}(\hat{X}_o - \hat{X}_n) \right]$$

where

- A is the partial derivative matrix of the measurements
- $\hat{}$ respect to the parameters
- X is the vector of adjusted dipole parameters
- δy is the vector of residuals
- W is the weight matrix for the measurements
- Λ_o is the a priori parameter covariance matrix
- $\hat{X}_o$ is the a priori estimate of the parameters and the estimate at the $(n+1)^{st}$ iteration is:

$$\hat{X}_{n+1} = \hat{X}_n + \delta\hat{X}_{n+1} \ .$$

An iterative technique is required for this problem when scalar magnetometer data is utilized due to the non-linearity introduced for this data type. The inversion problem is linear, however, for B_r, B_θ, B_ϕ data.

The major program subroutines and their functions are as follows:

MAIN: Program driver. Calls routines to initialize all variables. Loops through the least squares iteration, calling for data and partials, and accumulates the normal matrix and right-hand-side. Calls for inversion of normal matrix. Calculates updated parameter vector and statistics. After last iteration calculates statistics of data set for the recovered solution.

TSINV: Inverts a symmetric positive definite matrix stored row-wise in upper triangular form.

SETRHS: Initializes the right-hand-side to $\Lambda_o^{-1}(\hat{X}_o - \hat{X}_n)$ for each iteration when a priori information is used.

CLEAR: Sets arrays to zero values.

FUN: Computes the partial derivatives of B_r, B_θ, B_ϕ and B with respect to the parameters and calculates values for B_r, B_θ, B_ϕ, B in terms of current estimates of the parameters.

FUN2: Entry in FUN. Initializes the positions of dipoles on first call, establishing the size of equal area blocks to be used. Zeroes the normal matrix and right-hand-side on each call. Calculates the a priori covariance matrix when there are constraints for the orientation of the dipoles along specified directions.

FUN3: Entry in FUN. Calculates the angles between the solution dipoles and specified directions.

TMULT: Calculates the matrix $B \times B^T$.

FLD: Specifies a preferred direction for the dipoles.

EQAREA: Positions the dipoles at the center of equal area blocks with optional angular separations of 64°, 32°, 21°, and 16°.

GNORML: Computes random numbers of specified mean and variance.

CORLPR: Prints solution normal, covariance and correlation matrices.

SVDATA: Inputs MAGSAT scalar and vector data from tape. Provides data B_r, B_θ, B_ϕ, B for a particular time and position on each call.

SPHCOE: Computes spherical harmonic coefficients from the dipole parameters.

GSPACE: Assembly language routine which computes machine core memory size requirements dynamically.

BIAS: Computes the observatory anomaly biases on option when observatory annual means data is used.

SDATA: Inputs observatory and repeat data from tape.